

# COSIM - A Finite-Difference Computer Model to Predict Ternary Concentration Profiles Associated With Oxidation and Interdiffusion of Overlay-Coated Substrates

James A. Nesbitt  
NASA Glenn Research Center  
Cleveland, OH 44135

## Abstract

A finite-difference computer program (COSIM) has been written which models the one-dimensional, diffusional transport associated with high-temperature oxidation and interdiffusion of overlay-coated substrates. The program predicts concentration profiles for up to three elements in the coating and substrate after various oxidation exposures. Surface recession due to solute loss is also predicted. Ternary cross terms and concentration-dependent diffusion coefficients are taken into account. The program also incorporates a previously-developed oxide growth and spalling model to simulate either isothermal or cyclic oxidation exposures. In addition to predicting concentration profiles after various oxidation exposures, the program can also be used to predict coating life based on a concentration dependent failure criterion (e.g., surface solute content drops to 2%). The computer code is written in FORTRAN and employs numerous subroutines to make the program flexible and easily modifiable to other coating oxidation problems.

## Introduction

Many blades and vanes in gas turbine engines are coated with an aluminide or overlay coating to impart additional oxidation and corrosion protection to the component. These coatings provide protection by the selective oxidation of Al to form a compact and adherent  $\text{Al}_2\text{O}_3$  scale. Under isothermal conditions, the  $\text{Al}_2\text{O}_3$  scale thickens at a parabolic rate (scale thickness proportional to the square root of time). Diffusional transport within the coating supplies Al to the growing oxide scale at a rate consistent with the parabolic growth of the scale. Although Al is continually consumed from the coating, the rate is acceptably low such that the coating typically contains sufficient Al to easily provide protection during isothermal oxidation conditions. Although land-based turbines often operate in a nearly isothermal mode for long periods, aero gas turbines undergo thermal cycling with each flight. This thermal cycling, primarily to ambient temperatures when the engine is shut down, can cause cracking and partial spalling of the protective  $\text{Al}_2\text{O}_3$  scale. This spallation generally occurs randomly across flat component surfaces but is higher at edges and corners. The spalling may occur to the metal surface but more commonly occurs only in the outer layers of the oxide scale. However, loss of the oxide is not catastrophic since selective oxidation of Al continues when the component again reaches high temperatures such that the damaged scale will "heal" and continue to grow. Whenever scale spallation occurs due to thermal cycling during oxidation (i.e., cyclic oxidation), the oxide scale on the surface will, on average, be thinner than a scale grown isothermally for

equivalent hot exposure times. Since the rate of scale growth is inversely proportional to the scale thickness, a consequence of this thinner oxide scale is that the average rate of Al consumption is greater during cyclic oxidation accompanied by scale spallation than during isothermal oxidation. Hence, Al is depleted from the coating at a higher rate during cyclic oxidation, the exact rate depending on the growth rate of the alumina scale and the amount of oxide spalling. This paper will focus specifically on degradation of MCrAlY overlay coatings, where M stands for either Ni, Co or Fe. These coatings are often used on components in marine environments where hot corrosion protection is required, and in military applications where higher temperatures are often encountered.

In addition to oxidative attack, overlay coatings are further degraded by interdiffusion with the substrate. Since the coating is, by nature, higher in Al content than the substrate, Al diffuses from the coating into the substrate and generally becomes unavailable to support the growth of the protective alumina scale. Likewise, the Cr concentration in the coating is also typically greater than that in the substrate resulting in the diffusion of Cr from the coating into the substrate. In contrast, Ni and other elements in the substrate diffuse into the coating. Although the Y in the alloy strongly affects adherence of the Al<sub>2</sub>O<sub>3</sub> scale during cyclic oxidation, it is at such low concentration in the coating (e.g., <0.2 at.%) that dilution by interdiffusion with the substrate is generally not considered. Schematic concentration profiles in the coating and substrate after a short exposure in an oxidizing environment are shown in Fig. 1. When a coating is substantially depleted of Al during cyclic oxidation, it can no longer supply sufficient Al to re-heal the protective scale. Less protective oxides, such as NiO, FeO or CoO, can form signaling the end of the protective life of the coating. A critical Al content in the coating can be defined to indicate the useful life of the coating. This critical Al content could indicate the time at which less-protective oxides form on the surface, or an earlier time at which the coating could be stripped from the component and a new coating applied. Modeling the Al transport in the coating and substrate during cyclic oxidation allows the coating life to be predicted. The purpose of the present work was to develop a one-dimensional ternary diffusion model to predict the concentration profiles associated with the oxidation and interdiffusion of coated superalloys undergoing cyclic oxidation. This model, given the name COSIM for Coating Oxidation and Substrate Interdiffusion Model, employs finite-difference techniques embodied in a FORTRAN computer program to provide numerical solutions to the appropriate diffusion equations. The computer code employs numerous subroutines to make the program flexible and easily modifiable to other high temperature coating oxidation problems. Although the computer program and discussion below are primarily in terms of a NiCrAl coating on a Ni-based substrate, other elements could be substituted for the Al and Cr.

### **Ternary Diffusion Equations**

Because of the low Y content, MCrAlY overlay coatings can be approximated as ternary alloys with Al and Cr in a matrix of either Ni, Co or Fe. Ternary diffusion equations can be employed to simulate the Al and Cr transport associated with coating oxidation and coating/substrate interdiffusion. The choice of simulating Cr rather than Ni diffusion is inconsequential. In the ternary system, the concentration of the third component, being a dependent variable, is always determined by difference (i.e.,  $C_{Ni} = 100 - C_{Al} - C_{Cr}$ ). Since most superalloys are complex multicomponent, multiphase alloys, fully accounting for diffusional

interactions of the various superalloy components, as well as that of Y in the coating, on the Al and Cr transport is beyond current capabilities. Hence, these potential interactions, other than those encountered in the ternary system, are ignored. In addition, NiCrAlY and CoCrAlY overlay coatings generally consist of two phases, a high-Al NiAl or CoAl  $\beta$  phase embedded in a Ni or Co solid solution  $\gamma$  phase. This  $\beta$  phase is depleted as Al is consumed as oxide and as Al diffuses into the substrate. It has previously been shown that this  $\beta$  phase is often completely dissolved well before the useful life of the coating has been reached (Ref. 1). It was also shown in this same reference that good agreement was achieved between measured and predicted concentration profiles in the coating at extended times after the  $\beta$  phase had been dissolved by assuming a single-phase coating for the entire oxidation exposure. Hence, in the current model development, the two-phase coating will be represented as a single phase.

Fick's laws describing diffusion in a ternary alloy are:

$$J_j = -D_{j,j} \frac{\partial C_j}{\partial X} - D_{j,k} \frac{\partial C_k}{\partial X} \quad j, k = Al, Cr \quad \text{1st Law} \quad \text{Eq. 1}$$

and

$$\frac{\partial C_j}{\partial t} = \frac{\partial \left( D_{j,j} \left( \frac{\partial C_j}{\partial X} \right) \right)}{\partial X} + \frac{\partial \left( D_{j,k} \left( \frac{\partial C_k}{\partial X} \right) \right)}{\partial X} \quad j, k = Al, Cr \quad \text{2nd Law} \quad \text{Eq. 2}$$

where  $J_j$  is the flux of component  $j$ ,  $C$  is the concentration of either Al or Cr,  $D$  is one of the four ternary interdiffusion coefficients, or diffusivities, and  $X$  and  $t$  refer to distance and time, respectively. The first term on the right hand side (RHS) of Eq. 2 can be rewritten as:

$$\frac{\partial \left( D_{j,j} \left( \frac{\partial C_j}{\partial X} \right) \right)}{\partial X} = D_{j,j} \frac{\partial^2 C_j}{\partial X^2} + \frac{\partial D_{j,j}}{\partial X} \frac{\partial C_j}{\partial X} \quad j, k = Al, Cr \quad \text{Eq. 3.a.}$$

Equation 3.a can be further expanded as:

$$\frac{\partial \left( D_{j,j} \left( \frac{\partial C_j}{\partial X} \right) \right)}{\partial X} = D_{j,j} \frac{\partial^2 C_j}{\partial X^2} + \left( \frac{\partial D_{j,j}}{\partial C_j} \frac{\partial C_j}{\partial X} + \frac{\partial D_{j,j}}{\partial C_k} \frac{\partial C_k}{\partial X} \right) \frac{\partial C_j}{\partial X} \quad j, k = Al, Cr \quad \text{Eq. 3.b.}$$

A similar equation exists for the second term on the RHS of Eq. 2, namely:

$$\frac{\partial \left( D_{j,k} \left( \frac{\partial C_k}{\partial X} \right) \right)}{\partial X} = D_{j,k} \frac{\partial^2 C_k}{\partial X^2} + \left( \frac{\partial D_{j,k}}{\partial C_j} \frac{\partial C_j}{\partial X} + \frac{\partial D_{j,k}}{\partial C_k} \frac{\partial C_k}{\partial X} \right) \frac{\partial C_k}{\partial X} \quad j, k = Al, Cr \quad \text{Eq. 3.c.}$$

Substituting Eqs. 3.b and 3.c into the two terms on the right hand side of Eq. 2 yields:

$$\frac{\partial C_j}{\partial t} = D_{j,j} \frac{\partial^2 C_j}{\partial X^2} + \left( \frac{\partial D_{j,j}}{\partial C_j} \frac{\partial C_j}{\partial X} + \frac{\partial D_{j,j}}{\partial C_k} \frac{\partial C_k}{\partial X} \right) \frac{\partial C_j}{\partial X} +$$

$$D_{j,k} \frac{\partial^2 C_k}{\partial X^2} + \left( \frac{\partial D_{j,k}}{\partial C_j} \frac{\partial C_j}{\partial X} + \frac{\partial D_{j,k}}{\partial C_k} \frac{\partial C_k}{\partial X} \right) \frac{\partial C_k}{\partial X} \quad j,k = Al, Cr \quad \text{Eq. 4.}$$

Initially, transport associated with oxidation and the interdiffusion of the coating and substrate may be viewed as independent problems. Hence, at short times, coating/substrate interdiffusion can be treated as interdiffusion between two semi-infinite materials at a location centered on the coating/substrate interface. Similarly, oxidation of the coating can be treated as oxidation of a semi-infinite material affecting only a thin region below the surface of the coating. These two regions, the “inner” diffusion zone resulting from coating/substrate interdiffusion and the “outer” diffusion zone resulting from transport associated with oxidation, are shown schematically in Fig 2. At longer times, the two diffusion zones will overlap and diffusion associated with the two regions must be considered together. A solution to Fick’s second law (Eq 2), whether analytical or numerical, requires initial and boundary conditions. The boundary condition at the oxide/coating interface is discussed in the following paragraphs whereas the initial conditions and other boundary conditions used by the COSIM model are discussed in a later section.

For isothermal oxidation, the boundary condition at the oxide/coating interface, given as the rate of Al consumption, is well defined and decreases uniformly with time (the time dependence of the rate is inversely proportionate to the square root of time). However, for cyclic oxidation, the rate of Al consumption can vary in a non-uniform manner as the thickness of the oxide scale increases during the high temperature exposure but decreases on cooling as spallation occurs (Ref 2). In the present diffusion model, a separate model simulating oxide growth and spallation during cyclic oxidation has been adopted to provide the oxide/coating boundary condition. This oxide growth and spalling model (Ref 3), designated COSP by the authors, predicts the rate of Al consumption during each cycle by continuously tracking the thickness of the oxide scale, accounting for growth during high-temperature exposures, and partial oxide loss on cooling. This rate of Al consumption ( $J_{ox}$ ) predicted by COSP is used as the boundary condition for the diffusion model. Hence, the supply of Al within the coating to the oxide/coating interface must equal  $J_{ox}$ . However, since Al is consumed from the coating, the coating surface recedes due to the loss of matter. This recession ( $\xi$ ) is given as (Ref 4):

$$\xi = -V_{Al} J_{ox} t \quad \text{Eq. 5}$$

where  $V_{Al}$  is the partial molar volume of Al in the coating and  $J_{ox}$  is the rate of Al consumption discussed above (which is also the flux of Al entering the oxide).  $J_{ox}$  can also be considered as the Al flux to the left of the moving oxide/metal interface in Fig 2, or the Al flux *away from* the interface. Similarly,  $J_{Al}$  is the flux in the metallic coating *towards* the interface. Because of the interface motion,  $J_{ox}$  is greater than  $J_{Al}$  according to the relationship:

$$J_{ox} \Big|_{X=\xi^-} = \alpha J_{Al} \Big|_{X=\xi^+} \quad \text{Eq. 6}$$

where  $\xi^-$  and  $\xi^+$  refer to the left hand side and right hand side of the oxide/coating interface, respectively, as shown in Fig 2. The parameter  $\alpha$  in Eq. 6 is given as:

$$\alpha = \frac{1}{(1 - V_{Al} * C_{Al,0})} \quad \text{Eq. 7}$$

where  $C_{Al,0}$  is the Al concentration in the coating at the oxide/coating interface (Fig 2). Obviously, for the hypothetical case for  $V_{Al}=0$  (the Al atoms in the coating have no volume),  $\alpha=1$ , the Al flux to the interface,  $J_{Al}$ , becomes equal to the Al flux away from the interface,  $J_{ox}$ , and the interface is stationary. The partial molar volume for Al was assumed independent of concentration due to a lack of available data for most alloy systems of interest (e.g., the  $\gamma$ , Ni solid solution phase in NiCrAl alloys).

Hence, the boundary condition for Al at the oxide/coating interface is given by Eq. 6 whereby the rate of Al consumption due to oxide formation, predicted by the COSP oxide model,  $J_{ox}$ , is equated to the supply, or flux, of Al to the interface within the coating,  $J_{Al}$ , while taking into account the motion of the interface through the parameter  $\alpha$ . The rate of Al transport within the coating to the oxide/coating interface (i.e., the Al flux,  $J_{Al}$ ) is given by Eq. 1, stated as:

$$J_{Al} \Big|_{x=\xi^+} = -D_{Al,Al} \frac{\partial C_{Al}}{\partial X} - D_{Al,Cr} \frac{\partial C_{Cr}}{\partial X} \quad \text{Eq. 8}$$

Although no Cr is assumed to enter the  $Al_2O_3$  scale, the surface recession requires the diffusion of Cr and Ni away from the oxide/coating interface into the coating. The boundary condition for Cr is:

$$J_{Cr} \Big|_{x=\xi^+} = -D_{Al,Cr} \frac{\partial C_{Al}}{\partial X} - D_{Cr,Cr} \frac{\partial C_{Cr}}{\partial X} = C_{Cr,0} \frac{d\xi}{dt} \quad \text{Eq. 9}$$

where  $J_{Cr}$  is the flux of Cr in the coating away from the interface and  $C_{Cr,0}$  is the Cr concentration in the coating at this interface (Fig 2). In the computer program, the calculations for COSP have been contained in a subroutine to facilitate the incorporation of other oxide growth and spalling models (e.g., Ref 5).

### Finite-Difference (F-D) Method

The initial step in the F-D technique is to establish a grid of equispaced nodes across the region of the material over which diffusion will occur (i.e., the diffusion zone). Each node has a specific concentration associated with it. Fick's laws (Eqs. 1 and 4) are replaced with F-D equivalents based on small differences in concentration,  $\Delta C$ , distance,  $\Delta X$ , and time,  $\Delta t$ . A solution yielding the concentration profile at some time  $t$  is derived by solving the appropriate F-D equivalents for small time increments ( $\Delta t$ ) in an iterative manner. These iterations, or time steps, are continued until the  $\Delta t$  increments sum to the desired time  $t$ . A portion of a diffusion zone at time  $t$  and the new concentrations at time  $t+\Delta t$  is shown schematically in Fig 3 (Ref 6). Because of the typically large number of repetitive and tedious calculations made each iteration, F-D solutions are ideally handled by a computer.

The F-D equivalents to Fick's laws are based on Taylor series expansions (Refs 7,8). The F-D equivalent of Fick's 2nd law (Eq. 4) can be given by either an explicit or implicit

representation. The explicit form was used throughout this work. F-D expressions for both first and second order partial derivatives for concentration with respect to distance, given on the right hand side of Eq. 4, were given by first central difference equations, stated as:

$$\frac{\partial C_j}{\partial X} = \frac{C_{j,n+1} - C_{j,n-1}}{2\Delta X} \quad \text{Eq. 10}$$

$$\frac{\partial^2 C_j}{\partial X^2} = \frac{C_{j,n+1}^i - 2C_{j,n}^i + C_{j,n-1}^i}{(\Delta X)^2} \quad \text{Eq. 11}$$

where  $j$  refers to either Al or Cr,  $n$  refers to the node number and the superscript  $i$  refers to the current iteration at time  $t$ . These equations apply to all nodes  $n$  where nodes  $n-1$  and  $n+1$  exist. A first forward difference expression was used for  $\partial C/\partial t$  in the left hand side of Eq. 4, given as:

$$\frac{\partial C_j}{\partial t} = \frac{C_{j,n}^{i+1} - C_{j,n}^i}{\Delta t} \quad j = Al, Cr \quad \text{Eq. 12}$$

where the superscript  $i+1$  refers to the next iteration at time  $t+\Delta t$ . The time increment  $\Delta t$  for the explicit F-D method is limited by a stability criterion typically given as:

$$D_{max} \frac{\Delta t}{(\Delta X)^2} \leq 0.25 \quad \text{Eq. 13.}$$

where  $D_{max}$  is the appropriate diffusion coefficient which is discussed in a later section. Although  $\Delta t$  is initially very small, the grid expansion scheme described below allows the time increment each iteration to increase, generally allowing long term simulation of oxidation with a reasonable number of program iterations.

The last terms in Eq. 4 to be discussed are the eight derivatives of the diffusion coefficients ( $\partial D/\partial C$ ). Obviously, the concentration dependence of the four ternary diffusivities is required to evaluate this expression. The concentration dependence of the diffusivities is input to the computer program in polynomial form. The computer program determines an abbreviated polynomial expression for each derivative using the polynomial coefficients. If some, or all of the ternary diffusivities are concentration independent, or if the concentration dependence is not known and cannot be input to the program, the value of the appropriate derivatives is zero. Hence, each of the terms on the right hand side of Eq. 4 have known values at time  $t$  and can be evaluated. Since  $\Delta t$  is determined from the stability criterion in Eq. 13 and values for  $C_{j,n}^i$  are known, values for  $C_{j,n}^{i+1}$  from the left hand side of Eq. 4 for the new time ( $t + \Delta t$ ) can be calculated.

For the boundary condition at the oxide/coating interface (Eqs. 8 and 9), no node exists in the oxide (i.e., no  $n-1$  node exists, where  $n$  is located at the interface) so that the central difference formulas in Eqs. 10 and 11 cannot be used. Consequently, concentration gradients ( $\partial C_j/\partial X$ ) at the interface were determined using second order forward difference equations. Hence, the F-D equivalent for the Al concentration gradient in both Eqs. 8 and 9 at the interface was given as:

$$\left. \frac{\partial C_{Al}}{\partial X} \right|_{X=\xi^*} = \frac{-C_{Al,2}^i + 4C_{Al,1}^i - 3C_{Al,0}^i}{2\Delta X} \quad \text{Eq. 14}$$

where the second subscript number refers to the node which is numbered sequentially from zero at the interface and the superscript refers to the current iteration at time  $t$  (i.e.,  $C_{Al,0}^i$  is the Al concentration in the coating at the oxide/coating interface,  $X=\xi^*$  shown in Fig 2). A similar expression was used for the Cr gradient. The diffusivities for Eqs. 8 and 9 were evaluated for the Al and Cr concentrations in the coating at the oxide/coating interface (i.e.,  $C_{Al,0}, C_{Cr,0}$ ). Substituting Eq. 14 into Eqs. 8 and 9 together with Eqs. 5-7 are sufficient to yield the interface concentrations  $C_{Al,0}^i, C_{Cr,0}^i$ .

### COSIM Computer Program

The COSIM program initially establishes separate diffusion zones for interdiffusion and oxidation. Typically, these diffusion zones are set to be very narrow (i.e., 0.1 micron) but are allowed to expand with increasing interdiffusion. When the diffusion zones eventually overlap within the coating, the two separate zones are combined and the simulation continues with a single zone across the coating and into the substrate. This approach allows the use of a reasonable number of nodes in a zone yet with a fine node spacing during the early times when the concentration gradients are steep. For greater accuracy, all variables used in the iterative calculations were defined as double precision.

The starting width of the outer and inner zones,  $DXCOAT$  and  $DXSUB$ , and the number of nodes in each zone,  $NCOAT$  and  $NSUB$ , respectively, are parameters input to the program. The spacing between nodes,  $DELX1$  for the outer zone and  $DELX2$  for the inner zone (i.e.,  $\Delta X$  in the F-D equations), is equal to the width of the zone divided by the number of nodes minus one (i.e.,  $NCOAT-1$  and  $NSUB-1$ , the minus one since both zones are bounded by nodes). The concentrations associated with each node for both diffusion zones are stored in arrays labeled 'Al' and 'Cr'. In the outer diffusion zone, the nodes are numbered sequentially starting with zero at the oxide/coating interface through  $NCOATH$  (equal to  $NCOAT-1$ ). The  $NSUB$  nodes in the inner diffusion zone are numbered from  $NSUBL$  (low) to  $NSUBH$  (high) with  $NSUBL$  starting at a value of  $NCOAT+2$ . Central difference equations, such as Eqs. 10 and 11, cannot operate on the endpoints of a zone since concentrations at nodes  $n+1$  and  $n-1$  are required. Although forward and backward difference expressions can be used at these locations, a common technique is to add ancillary nodes to the zone to allow the continued use of central difference equations. Hence, an additional ancillary node was added to the inner end of the outer diffusion zone and an ancillary node was added to each end of the inner diffusion zone ( $NSUBL-1$  and  $NSUBH+1$ ). The ancillary nodes maintain assigned constant concentration values. The node numbering scheme is schematically shown in Fig 4 for  $NCOAT=7$  (e.g., 7 nodes numbered 0 to 6) and  $NSUB=11$  (e.g., 11 nodes numbered 9 to 19). The ancillary node for the outer diffusion zone is shown as node 7 and the ancillary nodes for the inner diffusion zone are shown as nodes 8 and 20. As shown, different values for  $DXCOAT$  or  $DXSUB$ , or for  $NCOAT$  or  $NSUB$ , may result in different values for  $DELX1$  or  $DELX2$ .

## Initial Conditions

Initially, each of the nodes in the outer zone is assigned the concentration of the coating. The ancillary node (node 7 in Fig 4) maintains this coating concentration until the inner and outer diffusion zones overlap. These initial concentrations for the outer zone are shown in Fig 4. An error function solution was used to assign the coating and substrate compositions to the nodes in order to provide a smooth transition between the coating and substrate compositions. The *NSUBL* to *NSUBH* nodes in the inner zone are assigned concentrations as:

$$C_j = C_j^{coat} + (C_j^{sub} - C_j^{coat}) * \frac{1}{2}(1 + erf(X_{mod})) \quad j = Al, Cr \quad \text{Eq. 15}$$

where  $C_j^{coat}$ ,  $C_j^{sub}$  refer to the initial concentration of the coating and substrate, respectively and  $X_{mod}$  is a modified distance parameter ranging from -2 to +2 across the diffusion zone of width  $DXCOAT$ . This range in  $X_{mod}$  produces a smooth concentration gradient with end compositions within 0.5% of  $C_j^{coat}$ ,  $C_j^{sub}$ . The coating composition was assigned to the ancillary node at *NSUBL-1* (node 8 in Fig 4) and the substrate composition was assigned to the ancillary node at *NSUBH+1* (node 20 in Fig 4). Again, these ancillary nodes maintain these assigned concentrations until the diffusion zones overlap (i.e., the ancillary nodes are not operated upon by Fick's 2<sup>nd</sup> law, as discussed below). The initial concentrations for the inner diffusion zone are also shown in Fig 4.

Use of the error function solution to assign initial concentration values does not have a significant effect on later concentration values because of the small initial diffusion zone width and the small initial time increments. A value on the order of 0.1 microns was typically used for the initial diffusion zone width,  $DXSUB$ . Typically, 30 to 40 nodes are assigned to the zone so that the node spacing ( $\Delta X$ ) is 0.0025 to 0.003 microns. Substituting this latter value into Eq. 13 and using a typical value of  $10^{-10}$  cm<sup>2</sup>/s for  $D_{max}$  yields a time increment  $\Delta t$  of only 0.000225 seconds. Hence, hundreds to thousands of iterations will typically be performed before the first minute of simulated exposure time allowing ample iterations for the starting concentrations to adjust to satisfy Fick's 2<sup>nd</sup> law (Eqs. 2-4). Fortunately, when diffusion begins to affect the concentration at the ends of the zones, either at node *NCOATH*, *NSUBL* or *NSUBH*, the node spacings are allowed to expand (as shown in the following section) so that larger time increments can be used each iteration. Since the outer and inner zones may have different node spacings, the program determines the maximum diffusion coefficient ( $D_{max}$  in Eq. 13) for either the coating or substrate composition and uses the smaller of the two node spacings to determine the smallest time increment,  $DEL T$  (i.e.,  $\Delta t$  in the F-D equations), according to Eq. 13.

## Surface Recession, Flexible Zones and Semi-Infinite Boundary Conditions

The COSIM model utilizes a flexible grid technique to account for surface recession and to simulate the semi-infinite boundary conditions. As the outer surface recedes due to Al loss, the entire outer zone is shifted and the concentrations at each node are adjusted. The technique used to accomplish this shift and adjustment is referred to as a "Murray-Landis" (M-L) transformation (Ref 9). This transformation shifts the nodes an amount proportional to their position from the moving boundary ( $X=\xi$ ) to maintain a uniform node spacing. The semi-infinite boundary condition for the outer diffusion zone can be stated as:

$$C_i \Big|_{x=\infty} = C_i^{coat} \quad i = Al, Cr.$$

This boundary condition is approximated by increasing the zone width whenever diffusion “significantly changes” the concentration at the node *NCOATH*. Each iteration, the concentration at this node is changed slightly in accordance with Fick’s 2<sup>nd</sup> law (Eq. 4). A “significant change” used in the COSIM program was taken as 0.005 at.%. Varying this value from 0.002 to 0.008 at.% changed the number of iterations required to reach a fixed time but had no significant effect on the predicted concentration profiles at short or long times (i.e., 1 and 1000 hrs using the sample input data given in Appendix A). Hence, whenever the concentration of node *NCOATH* (either Al or Cr) varied from the coating composition by 0.005 at.%, the zone width was expanded by *DELX1* and all node positions and concentrations were adjusted according to the M-L transformation. To further illustrate this operation, Al loss at the surface (node 0) and operation of Fick’s 2<sup>nd</sup> law (Eq. 4) will eventually cause the initial Al profile in the outer diffusion zone (Fig 4) to appear as shown schematically by the solid squares in Fig 5. Eventually, the Al concentration at node 6 will decrease to a value 0.005 at.% below the concentration of the coating,  $C_{Al}^{coat}$ . During this iteration, the total zone width, *DXCOAT*, will be increased by an amount equal to the node spacing such that:

$$DXCOAT' = DXCOAT + DELX1 \quad \text{Eq. 16}$$

The number of nodes remains constant but the new node spacing is given as:

$$DELX1' = DXCOAT' / (NCOAT - 1) \quad \text{Eq. 17}$$

The node positions are shifted proportionately such that node 6 is shifted inward by *DELX1* while node 0 at the surface ( $X = \xi$ ) undergoes no shift (Fig 5). The concentrations at each node are shifted in a similar manner with node 6' taking the old position of the ancillary node 7 and being reassigned the concentration of the coating,  $C_i^{coat}$  (the concentration previously held by the ancillary node 7 at the same position). The ancillary node maintains the coating composition at the new position.

The semi-infinite boundary conditions at either end of the inner diffusion zone are simulated in a like fashion. Hence, as diffusion changes the concentrations at nodes *NSUBL* or *NSUBH* in the inner diffusion zone by 0.005 at.%, the zone width is expanded by the node spacing, *DELX2* and the node positions and concentrations are adjusted according to the M-L transformation. The expansion occurs at the end of the zone where the concentration change occurred such that the inner diffusion zone expands either into the coating or into the substrate for changes at node *NSUBL* or *NSUBH*, respectively. The ancillary nodes (*NSUBL-1* and *NSUBH+1*) maintain the substrate composition and are repositioned at the ends of the zones with the new node spacing. Whenever the zones are expanded or contracted, a new time increment *DELTA*, is calculated according to Eq. 13. As discussed above, the smaller of the time increments calculated for the outer and inner diffusion zones is always used. Because of the concentration dependence of the diffusivities, one end of the inner diffusion zone may expand more than the other over the course of several thousand iterations. Although the inner and outer zones may appear very different with different widths, different numbers of nodes and different node spacings, both zones always operate with the same time increment such that the total exposure time for both the inner and outer diffusion zones is always identical.

The expansion of the inner and outer zones will eventually result in their impingement, or overlap, within the coating. From this time onward, the two diffusion problems, oxidation and coating/substrate interdiffusion, become coupled and can no longer be operated independently. At the time that the diffusion zones overlap, the COSIM model sums the current width of the inner and outer zones and redefines a single zone of equal width. Equidistant node spacings are also calculated using the combined number of nodes from the two zones (i.e.,  $N_{COAT} + N_{SUB}$ ). The COSIM model then fits a natural cubic spline curve (Ref 10,11) through the concentration profiles from both zones and generates a single profile through the coating and into the substrate for both Al and Cr at each of the new node positions. Figure 6a shows predicted Al and Cr concentration profiles in the coating and substrate at the time (time=1.34 hrs) when the two diffusion zones overlap. The width of the inner diffusion zone is significantly larger with a larger number of nodes and a larger node spacing than that for the outer diffusion zone. Figure 6b shows the same data after the spline interpolation. Note that the nodes are equally spaced across the entire diffusion zone. The spline subroutines are based on equations and code given in Ref 11. Following the combination of the two diffusion zones, the COSIM model continues to simulate Al transport to the surface and interdiffusion of the coating and substrate. Both boundary conditions, at the oxide/coating interface and in the substrate remain as before the combination. Loss of Al continues to cause surface recession and a shrinking of the zone while diffusion in the substrate continues to result in zone expansion. Within the program, the transition from two zones to one is reflected in the value of the parameter *ZONE*. The value of *ZONE* changes from two to one after the diffusion zones are combined and the program operates on the single diffusion zone thereafter. Parameters are redefined so that the new, single diffusion zone utilizes parameters associated with the outer diffusion zone (e.g., *DELX1*, *DELTI*, etc.) The model continues to simulate increasing oxidation exposure with each iteration of time. The program can print out concentration data at intermediate times (e.g., 50, 100, 500, 1000, 5000 hrs) or at some predetermined failure condition (e.g.,  $C_{Al,0} = 0$  or 5 at.%). Output is also written to files to ease plotting concentration/distance profiles. Figure 7 shows predicted concentration profiles after 1, 100 and 1000 hrs using the data given in Appendix A. Figure 8 shows the time dependence of the surface concentrations  $AL(0)$ ,  $CR(0)$ , rate of Al consumption and total weight of Al consumed which are also written to output files. Diffusivities for these examples were taken from reference 12. The value for the partial molar volume of Al was taken from reference 13.

Occasionally, oscillations in the values of the Al concentration at the oxide/coating interface,  $AL(0)$ , will occur the first few cycles. These oscillations can cause the computed value for the  $AL(0)$  to become negative or to exceed 100 at.%. It has also been observed that a very high initial flux from the COSP oxide growth and spalling model can also cause the computed value for  $AL(0)$  to be negative for hundreds of cycles. To protect against this physical impossibility, the program limits the values of  $AL(0)$  to be between 0 and 100 at.% (i.e., negative values are set equal to zero and values greater than 100 are set equal to 100). The consequence of these limits is that Eq. 6 is not satisfied during these iterations. However, monitoring the computed values for  $AL(0)$  typically show convergence to acceptable values at relatively short times (i.e., less than one hour when unreasonably high values for  $K_p$  were used with the example

input data given in Appendix A). Since these early oscillations could falsely trigger the test for  $AL(0)$  less than a critical Al concentration (i.e.,  $AL(0) \leq CRITAL$ ) this test is not initiated in the program during the first two hours of oxidation exposure. No problems have been encountered using test cases using various values for  $CRITAL$ , including zero.

Certain constraints on the time increment used each iteration ( $DELTA$ ) are desirable when simulating certain oxidation conditions. For instance, a value for  $DELTA$  much less than one hour might be desirable during cyclic oxidation with one hour cycles. In this case, a value of  $DELTA$  of one or five minutes might be desired so that several iterations during oxide growth can be performed between periods of oxide spallation each cycle. In contrast, for isothermal oxidation for long periods, it might be preferable to have no constraint on the values for  $DELTA$  in order to minimize the number of iterations to reach a solution. To provide this flexibility, a maximum value for  $DELTA$  ( $MAXDT$ ) may be input to the program. The default condition within the program is that no constraint be made on  $DELTA$  beyond that given in Eq. 13.

### Program Application

The program has been used to predict both concentration profiles and coating life after cyclic oxidation of overlay coated substrates (ref 1,14). The COSIM program has also been used to perform parametric studies to examine the effect of coating thickness and coating and substrate composition on coating life (ref 1). Recently, the program was modified to examine the coating life extension due to the presence of a perfect diffusion barrier between the coating and substrate (ref 14).

The COSIM program was initially compiled and executed on mainframe computers and later revised for execution on a desktop PC. The current version of the program has been compiled with ANSI FORTRAN95.

A description of the main program and each of the subroutines, as well as flowcharts, is given in reference 15. A description of each of the input parameters, an alphabetical list of all program variables, a sample input file and the corresponding output files are also given in this reference.

### References

1. J.A. Nesbitt and R.W. Heckel, *Thin Solid Films*, **119**, 281, 1984.
2. J.A. Nesbitt, "Diffusional Aspects of the High-Temperature Oxidation of Protective Coatings", in *Diffusion Analysis & Applications*, Edited by A.D. Romig, Jr. And M.A. Dayananda, TMS, Warrendale, 1989, p. 307-324.
3. C.E. Lowell, C.A. Barrett, R.W. Palmer, J.V. Auping, and H.B. Probst, *Oxid. Met.*, **36**, 81, 1991.
4. J.A. Nesbitt, *J. Electrochem. Soc.*, **136**, 1518 (1989)
5. K.W. Chan, *Met. and Mat. Trans.*, **28A**, 411, 1997.
6. J.A. Nesbitt, *Oxid. Met.*, **44**, 309, 1995.
7. R.W. Hornbeck, *Numerical Methods* (Quantum Publishers, New York, 1975).

8. M.L. James, G.M. Smith, and J.C. Wolford, Analog and Digital Computer Methods, (International Textbook, Scranton, 1964)
9. D. Murray and F. Landis, *J. Heat Transfer*, **81**, 106, 1959.
10. L.W. Johnson and R.D. Riess, Numerical Analysis, Addison-Wesley, Reading, MA (1977).
11. J.H. Mathews, Numerical Methods for Mathematics, Science and Engineering, 2<sup>nd</sup> Ed. Prentice Hall, Englewood Cliffs (1992).
12. J.A. Nesbitt and R.W. Heckel, *Met. Trans.*, **18A**, 2075, 1987.
13. J.A. Nesbitt, NASA TM 83738, Cleveland, OH, 1984.
14. J.A. Nesbitt and Jih-Fen Lei, "Diffusion Barriers to Increase the Oxidative Life of Overlay Coatings" in *Elevated Temperature Coatings: Science and Technology III*, Edited by J.M. Hampikian and N.B. Dahotre, TMS, Warrendale, USA, 1999, p. 131-142.
15. J.A. Nesbitt, NASA TM-2000-209271, Cleveland, OH, USA, 2000.

## Appendix A.

Al concentration in the coating (at.%)	13.0
Cr concentration in the coating (at.%)	20.0
Al concentration in the substrate (at.%)	5.0
Cr concentration in the substrate (at.%)	10.0
Density of the coating (gm/cm <sup>3</sup> )	7.754
Partial molar volume of Al in the coating (cm <sup>3</sup> /mole)	7.1
Coating thickness (microns)	100.0
Number of nodes in the "outer" coating diffusion zone	30
Number of nodes in the "inner" coating/substrate diffusion zone	40
Initial width of the outer diffusion zone (microns)	0.1
Initial width of the inner diffusion zone (microns)	0.1
Parabolic oxide growth parameter due to weight of oxygen in the oxide (mg <sup>2</sup> /cm <sup>4</sup> /hr)	0.002
The hot cycle duration for each thermal cycle, in hours.	1.0
The spall parameter for the COSP spalling model (Ref. 3)	0.008

The four ternary diffusion coefficients:

$$D_{AlAl}(C_{Ab}, C_{Cr}) = [1.229 + (0.0731 * C_{Al}) + (-0.0083 * C_{Cr}) + (0.0101 * C_{Al}^2) + (0.00016 * C_{Cr}^2)] * 10^{-10}$$

$$D_{AlCr}(C_{Ab}, C_{Cr}) = [0.0116 + (0.0923 * C_{Al}) + (-0.0010 * C_{Cr}) + (0.00016 * C_{Al}^2) + (0.000017 * C_{Cr}^2)] * 10^{-10}$$

$$D_{CrAl}(C_{Ab}, C_{Cr}) = [0.0766 + (-0.0153 * C_{Al}) + (0.0837 * C_{Cr}) + (0.00062 * C_{Al}^2) + (-0.0015 * C_{Cr}^2)] * 10^{-10}$$

$$D_{CrCr}(C_{Ab}, C_{Cr}) = [0.783 + (-0.0123 * C_{Al}) + (0.0247 * C_{Cr}) + (0.00096 * C_{Al}^2) + (-0.00057 * C_{Cr}^2)] * 10^{-10}$$

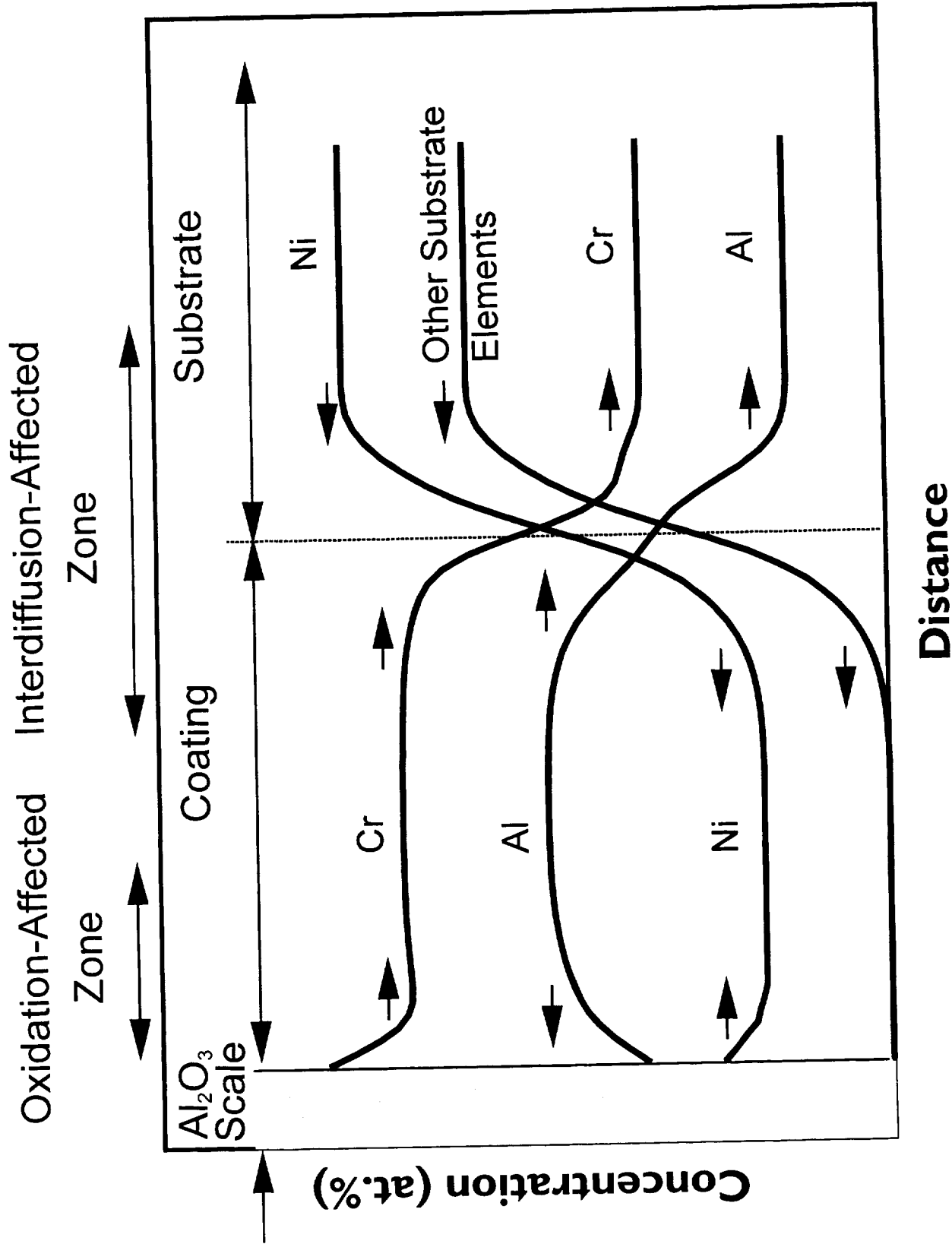


Figure 1. Schematic concentration profiles after oxidation exposure. Arrows indicate direction of atomic transport.

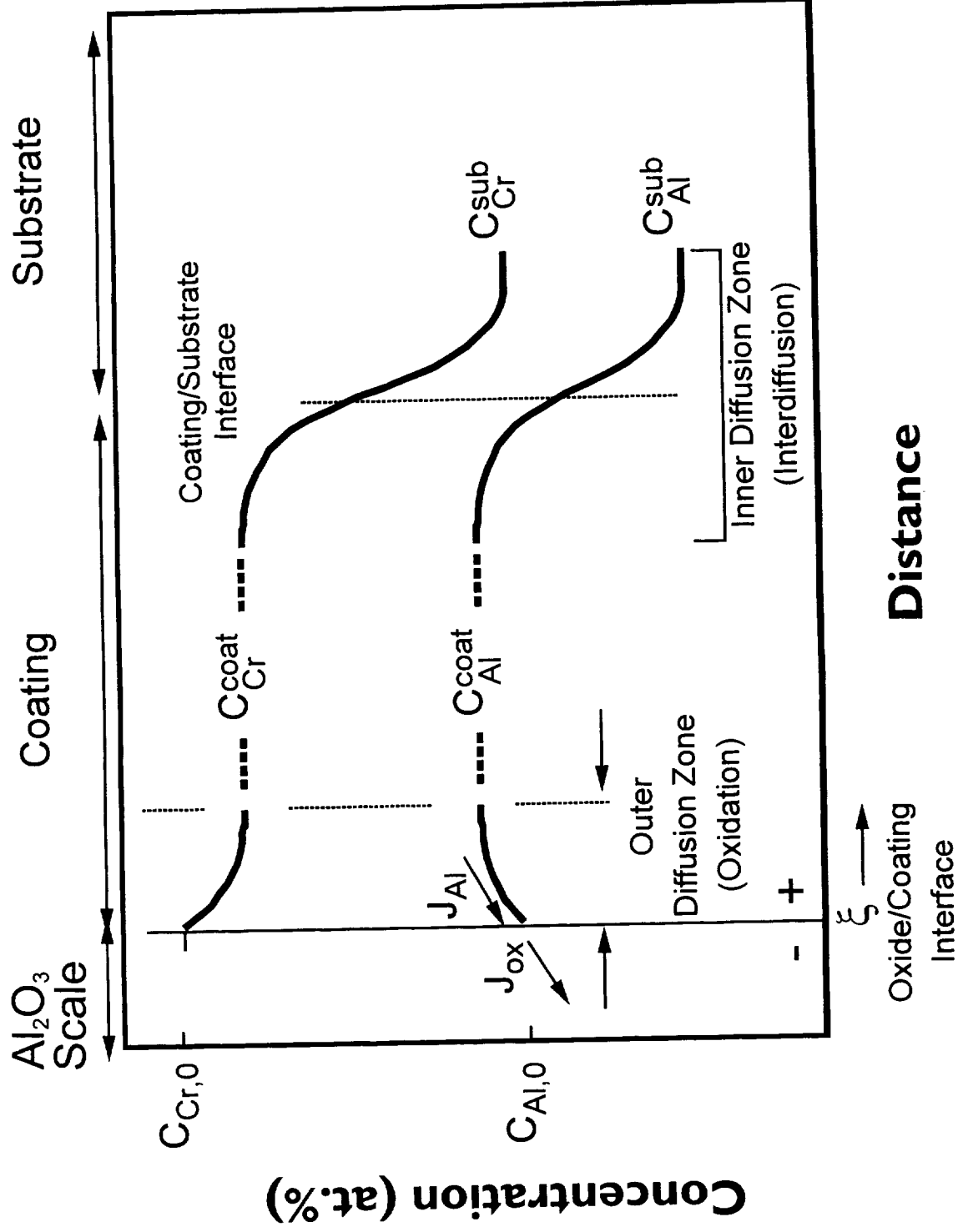


Figure 2 Schematic concentration profiles after a short oxidation exposure.

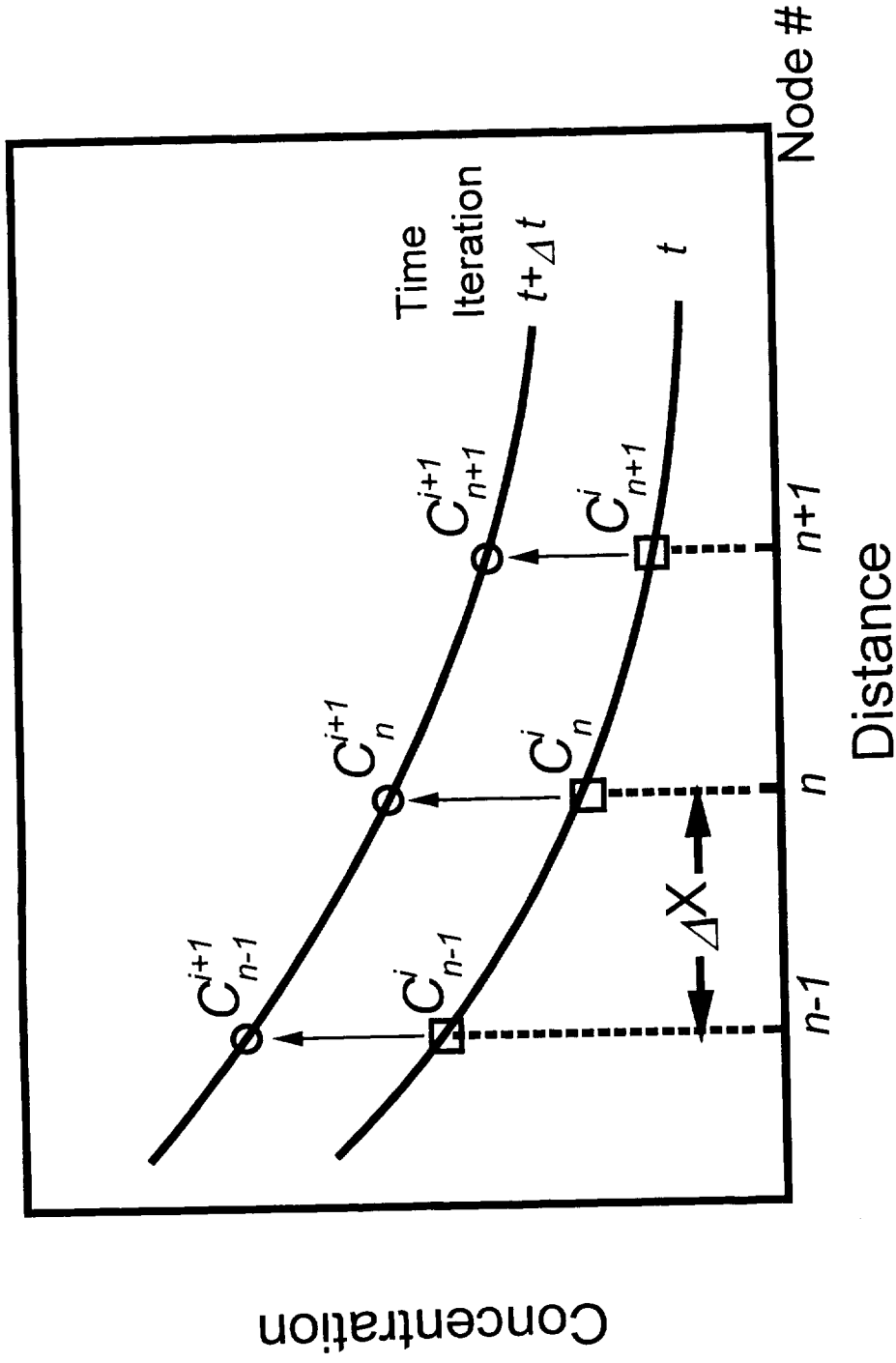


Figure 3. Schematic diffusion zone for time  $t$  (squares) and time  $t + \Delta t$  (circles). The concentration subscript refers to the node number and the superscript refers to the time iteration.

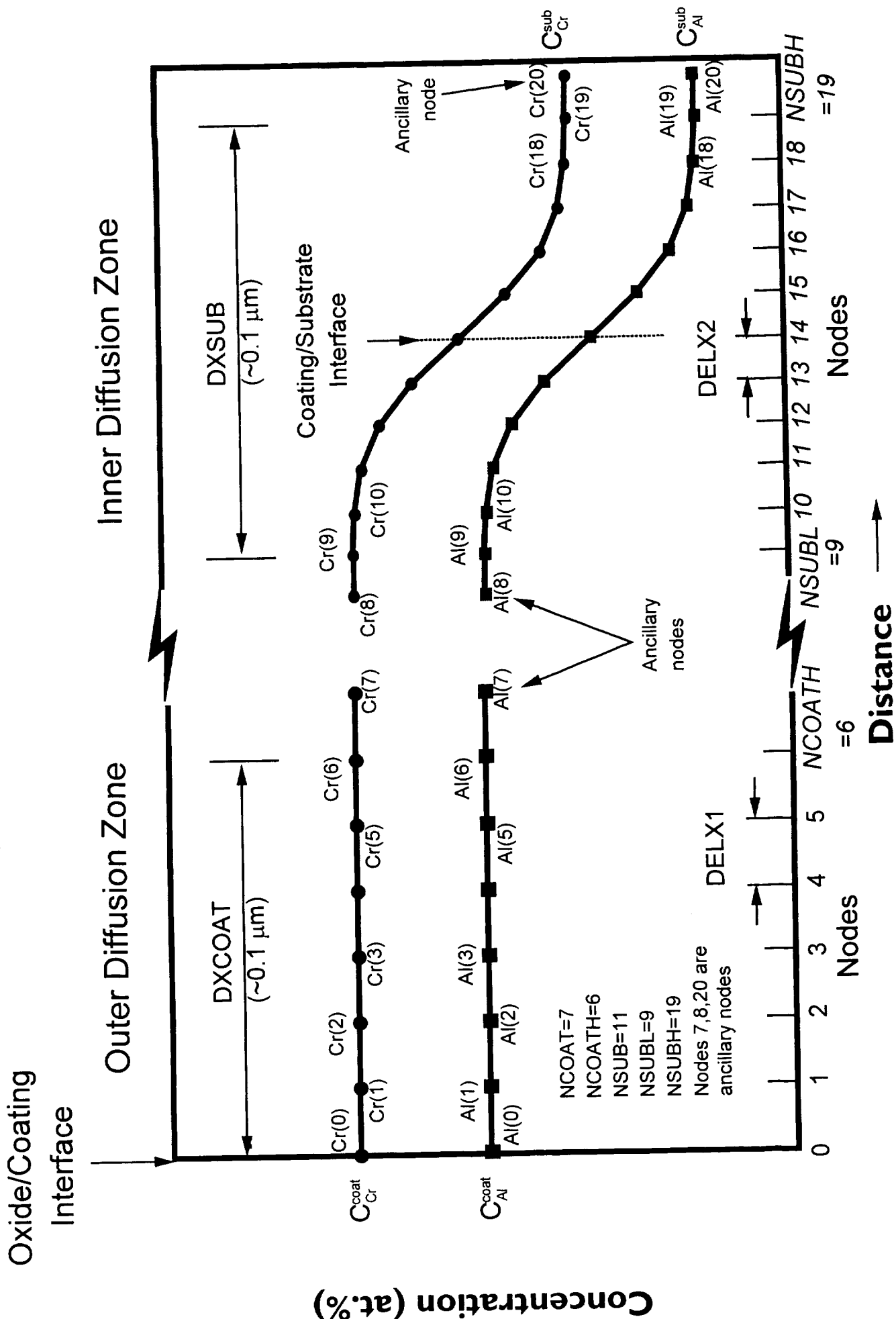


Figure 4. Schematic of initial concentration profiles before oxidation exposure for NCOAT=6 and NSUB=11.

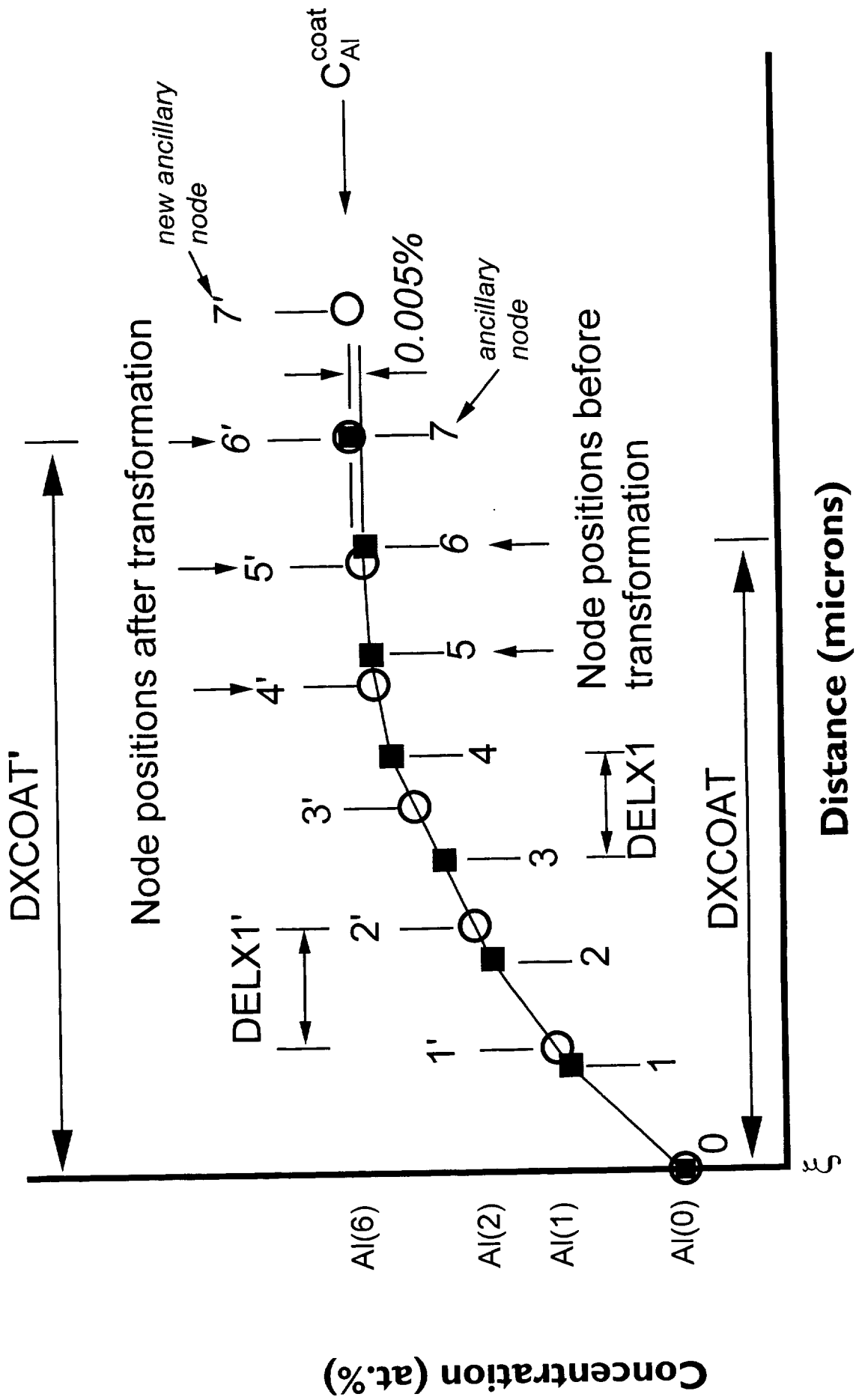


Figure 5. Schematic Al concentration profile in the outer diffusion zone before and after the M-L transformation.

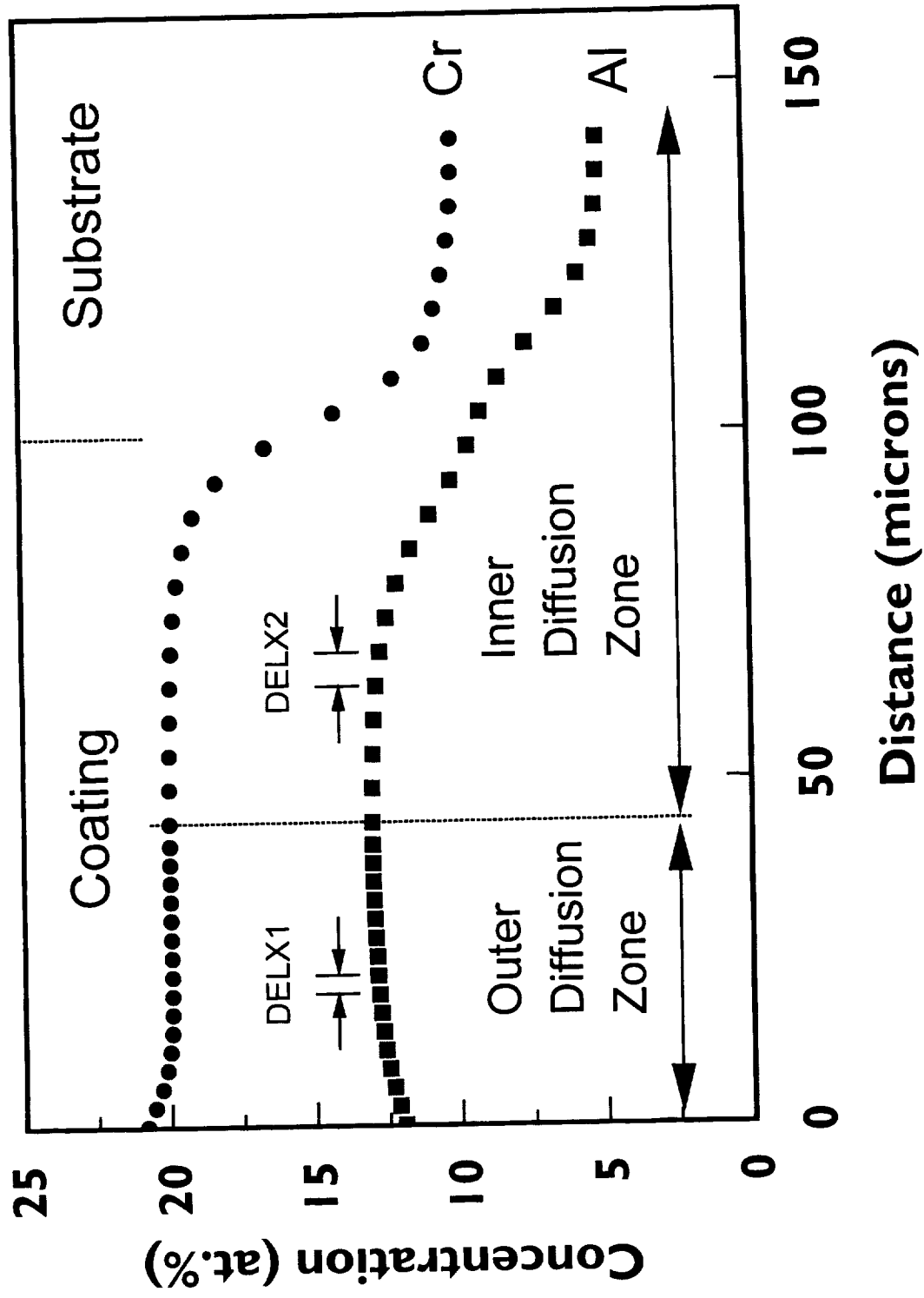


Figure 6a. Al and Cr concentration profiles at the time ( $time=1.34$  hrs) when the inner and outer diffusion zones overlap. Input data for run given in Appendix A. (Alternate nodes hidden for clarity.)

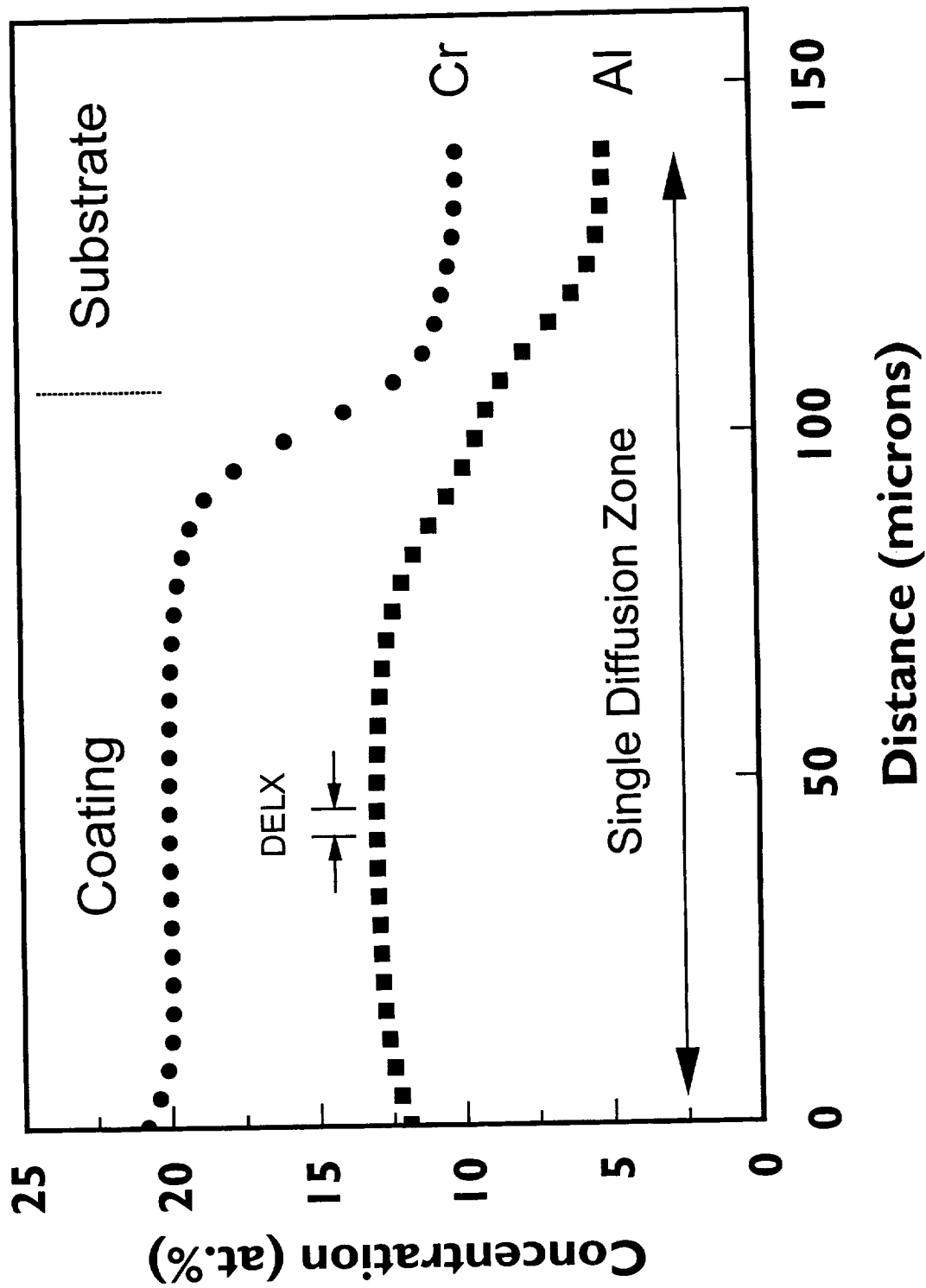


Figure 6b. Al and Cr concentration profiles at  $time=1.34$  hrs following the spline operation. Input data for run given in Appendix A. (Alternate nodes hidden for clarity.)

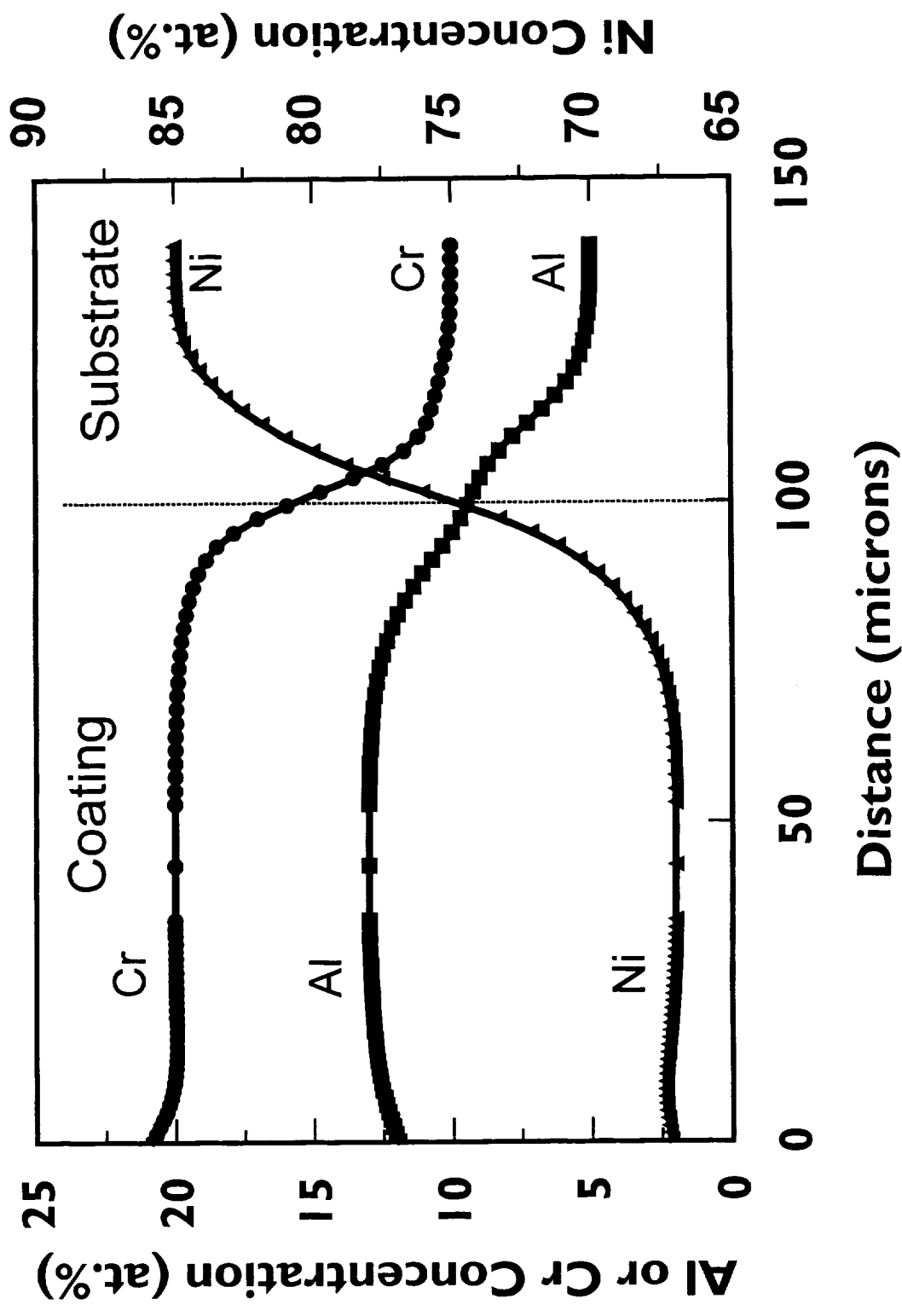


Figure 7a. Al, Cr and Ni concentration profiles at  $time=1.0$  hr using the input data given in Appendix A.

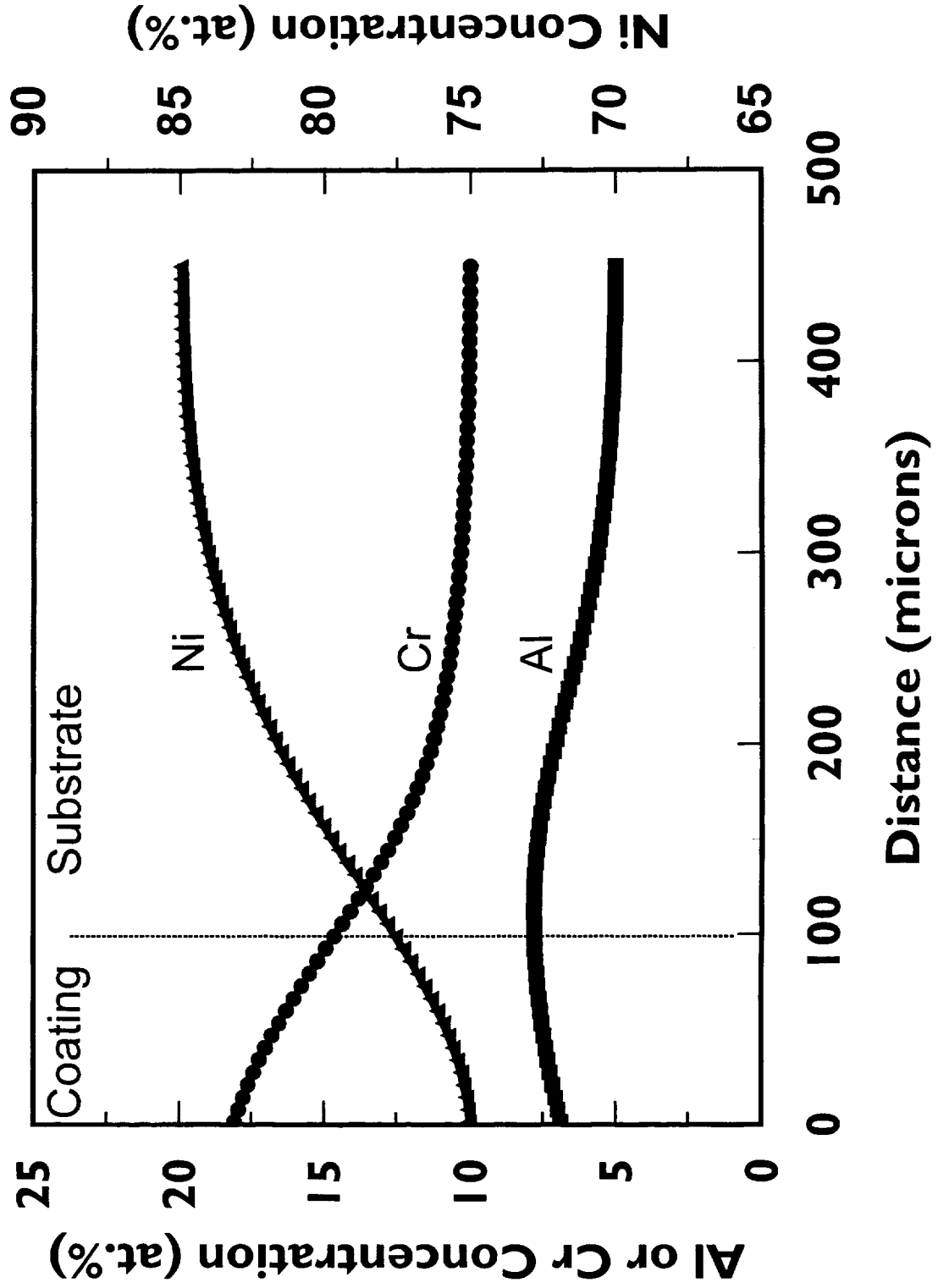


Figure 7b. Al, Cr and Ni concentration profiles at *time*=100.0 hrs using the input data given in Appendix A.

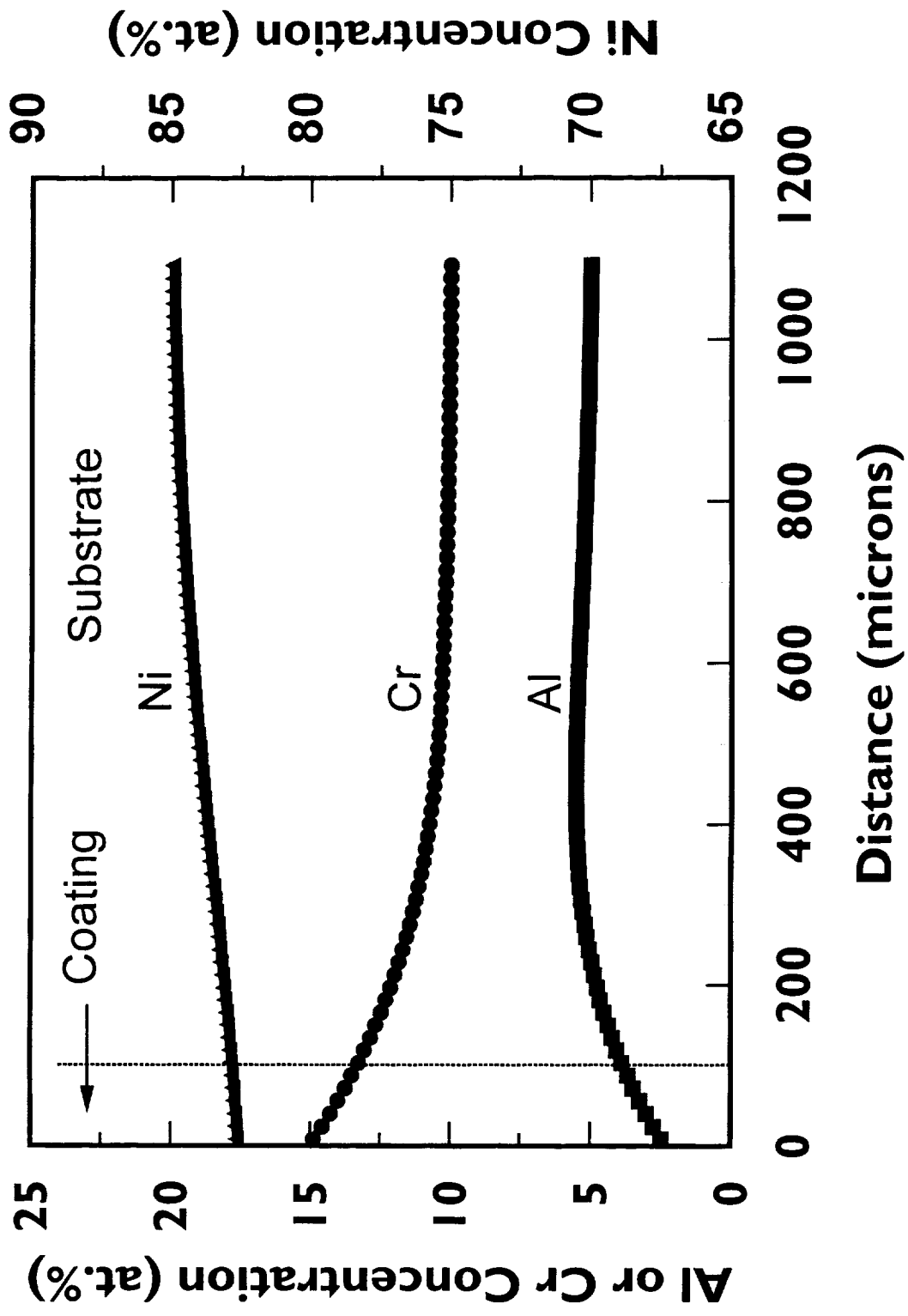


Figure 7c. Al, Cr and Ni concentration profiles at *time*=1000.0 hrs using the input data given in Appendix A.

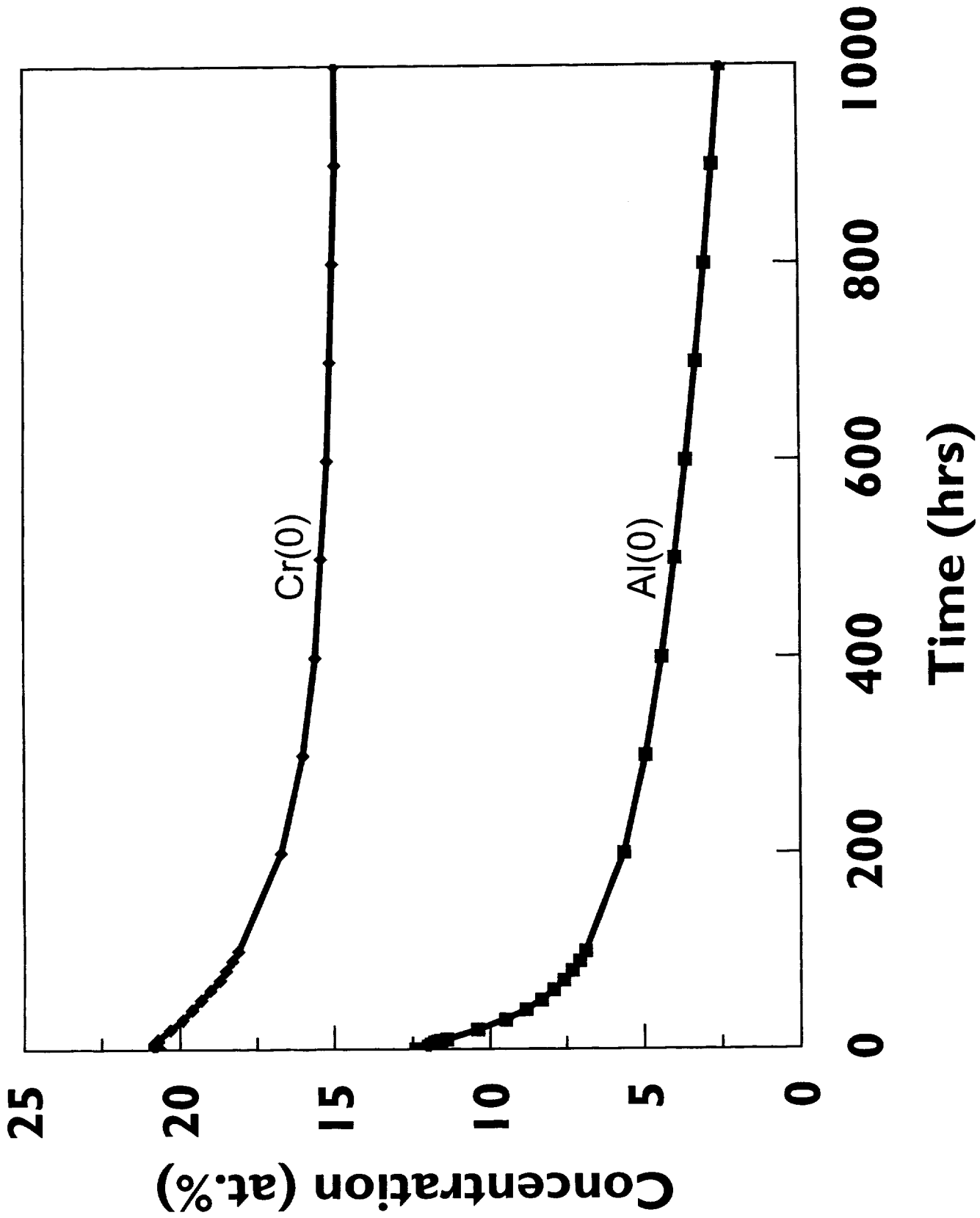


Figure 8a. Time dependence of Al and Cr concentrations at the surface (Al(0) and Cr(0)) from data written to unit 15 (File OUT15) for the input data given in Appendix A.

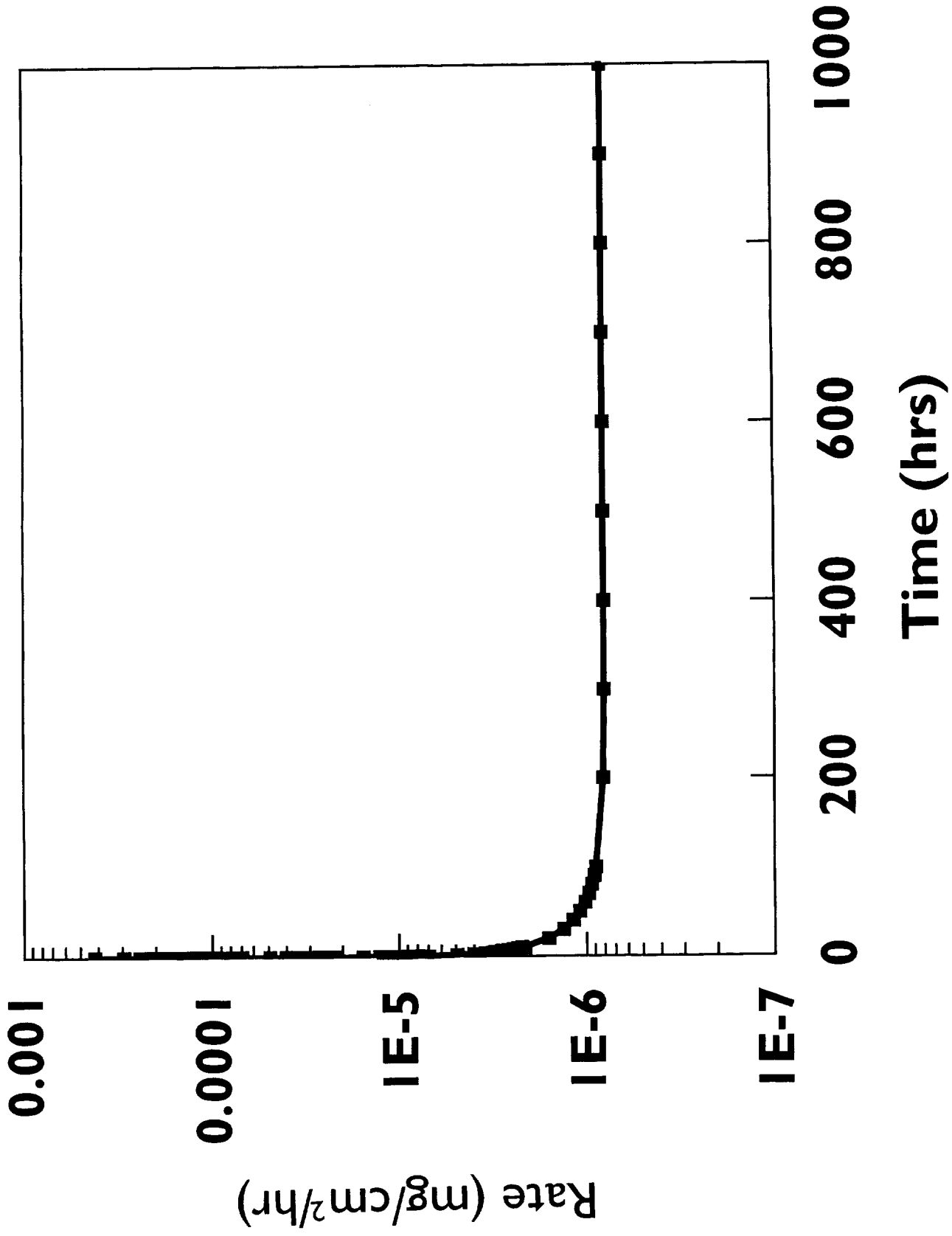


Figure 8b. Time dependence of WMDOT (rate of Al consumption) from data written to unit 15 (File OUT15) for the input data given in Appendix A.

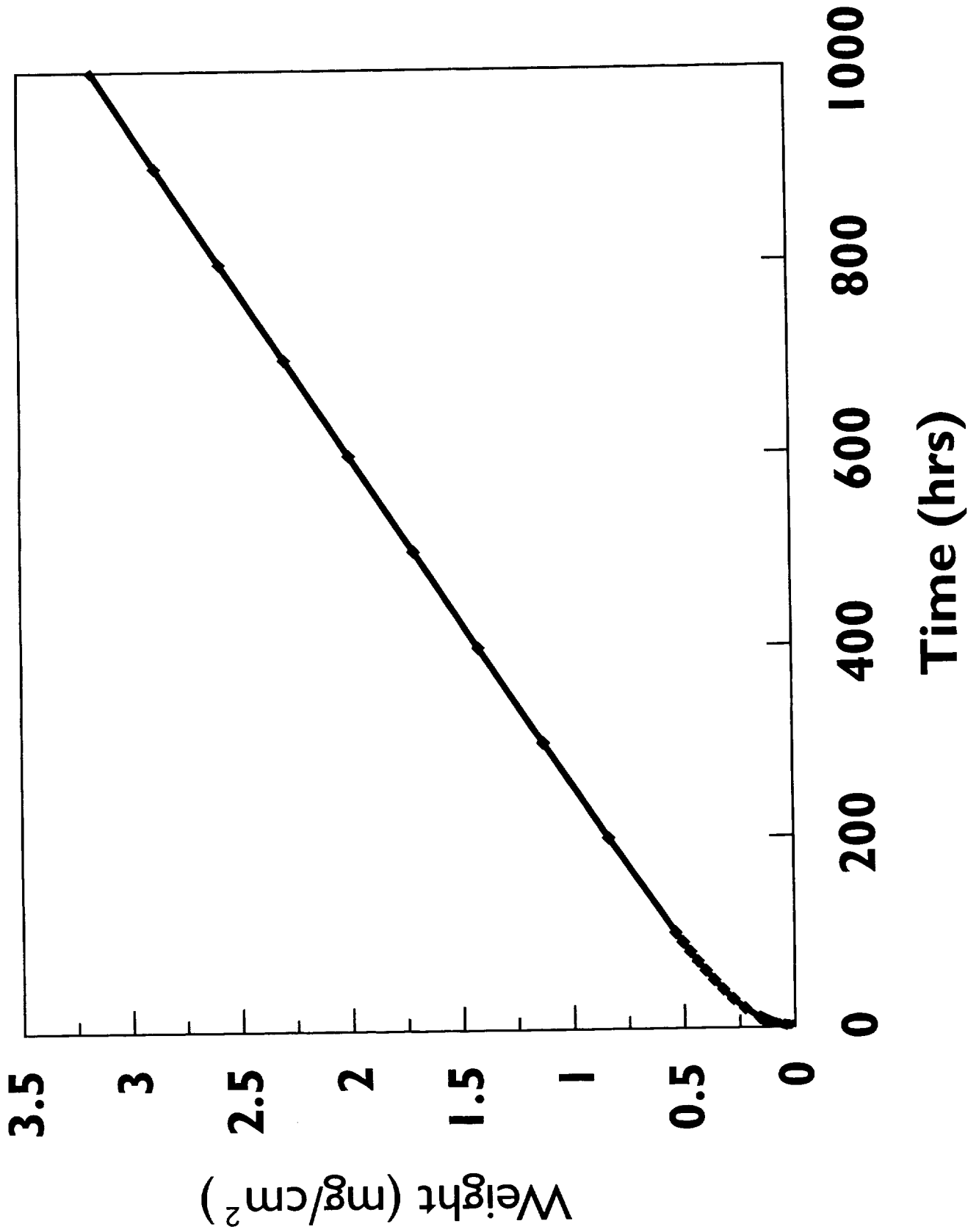


Figure 8c. Time dependence of WMINT (weight of Al consumed) from data written to unit 15 (File OUT15) for the input data given in Appendix A.